



# Development of metal oxide incorporated Al-Zn-Sn sacrificial anodes processed by stir casting and heat treatment

Abdelrahman Elsayed<sup>1</sup> · Adel Nofal<sup>2</sup> · Galal Attia<sup>1</sup>

Received: 22 April 2022 / Revised: 30 June 2022 / Accepted: 20 July 2022 / Published online: 25 August 2022  
© The Author(s) 2022

## Abstract

Aluminum sacrificial anodes are currently the first choice for cathodic protection in numerous applications. The galvanic performance of aluminum-based sacrificial anodes is considerably enhanced by addition of certain alloying elements called activators. Recent researches proved that incorporation of specific metal oxides like  $\text{MnO}_2$ ,  $\text{CeO}_2$ ,  $\text{RuO}_2$ , and  $\text{IrO}_2$  into the aluminum matrix could enhance the galvanic efficiency of aluminum anodes; however, the mechanism by which metal oxides improve galvanic properties of aluminum is still subject to discussion. The present work investigates the effect of incorporating commercially available low-cost manganese dioxide concentrate into Al-5Zn-0.1Sn sacrificial anodes in different volume fractions. It also studies the influence of heat treatment on anode's galvanic performance by performing solution treatment at 3 different temperatures (250 °C, 400 °C, 550 °C). The electrochemical testing results proved an increase in efficiency of anodes incorporated with metal oxides and solution treated at 550 °C. The SEM imaging and EDX elemental mapping declared that the presence of  $\text{SiO}_2$  particles in the anode matrix which might cause effective and uniform corrosion of Al anodes and decreased non-coulombic losses.

**Keywords** Sacrificial anodes · Cathodic protection · Galvanic efficiency · Aluminum metal matrix composites

## Introduction

Sacrificial anodes have been widely adopted as a reliable technique for cathodic protection in the last few decades and gradually superseded impressed current cathodic protection in numerous applications. This change in shares can be justified by several advantages of sacrificial anode systems over impressed current ones, e.g., there is no need for external power source which means unnecessary for overhead electrical infrastructure for remote areas, much easier installation, in addition to the significant advantage of the relatively low protection voltage and current between anode and surface to be protected so overprotection is unlikely to occur. Consequently, probability for occurrence of hydrogen embrittlement and coating disbonding due to hydrogen evolution is lower [1, 2].

Magnesium, zinc, and aluminum alloys are the main categories of sacrificial anodes used for cathodic protection systems. While magnesium is specifically used for unique type of applications, mainly protection of underground metallic structures like pipelines, aided by its high anodic potential which can overcome soil resistivity up to 5000  $\Omega$  cm [3], Mg sacrificial anodes cannot be used for applications in contact with seawater due to its high reactivity which implies undesired high self-corrosion rate that dramatically reduces current efficiency of the anode. On the other hand, zinc and aluminum are most suitable for marine applications due to the low resistivity of seawater medium, such as ship hulls, offshore pipelines, oil and gas production platforms, salt-water-cooled marine engines, ships' propellers, and rudders, and for protection of the internal surface of storage tanks.

Despite the fact that aluminum is superior to zinc in many advantageous properties, like its higher theoretical current capacity, 2980 A h/kg compared to 819 A h/kg for zinc, as well as its much smaller specific weight and lower cost. Zinc sacrificial anodes have been a more trustworthy option over aluminum anodes due to formation of passive oxide layer over aluminum, which acts as a barrier in the electrochemical interaction between anode and electrolyte

✉ Abdelrahman Elsayed  
a.elsayed@suezuni.edu.eg

<sup>1</sup> Faculty of Petroleum and Mining Engineering, Suez University, Suez, Egypt

<sup>2</sup> Central Metallurgical Research and Development Institute-CMRDI, Cairo, Egypt

medium. This oxide layer results into polarization of the anode reaching operation potential of  $-0.7$  V, which is not enough for structure protection and gradual stoppage of current supply from anode to the protected surface.

An extensive research work has been dedicated to improving the electrochemical performance of aluminum sacrificial anodes with a main target of preventing the formation of an adherent, continuous, and protective oxide layer ( $\gamma$ -Al<sub>2</sub>O<sub>3</sub>) on the surface of the alloy [4, 5], consequently permitting continuous charge transfer in sustaining galvanic activity of aluminum.

In 1966, Schrieber and Reding [6] developed a novel alloy of (Al–Zn–Hg) with mercury as an activator which gave superior galvanic efficiency of 95%, this alloy has been commercially available branded as (Galvalum I) [7].

In 2006, Bessone [8] showed that mercury in a concentration of less than 0.03% to Al base alloy caused a drastic breakdown of passive layer and lowered more than 0.3 V in its operational potential in chloride medium. This effect of Hg in solid solution is related to its role in disruption and co-dissolution of oxide surface assisting ion and charge transfer [9–12]. Despite this revolutionary performance, major concerns escalated on the effect of Hg on environment and marine life which inspired the development of several alternatives to be used as activators.

A comprehensive investigation made by Reding and Newport studied the effect of different alloying elements on operating potential of Al alloys as sacrificial anodes, e.g., Zn, Cd, Mg, and Ba were found to slightly decrease the potential. In, Hg, Sn, and Ga significantly decreased the potential at very low concentrations, and Mn and Cu were found to increase potential. However, Pb and Sb had no effect on potential [13].

Among the abovementioned elements, indium has been proved to substantially improve the electrochemical behavior of aluminum anodes which provided more negative operating potential ( $-1.08$  V) alongside high current capacity (2530 A h kg<sup>-1</sup>) with efficiency of 85% [14]. This new alloy was proposed to the market with trademark (Galvalum III) and started to gradually replace (Galvalum I) due to the environmental concerns on the latter.

Alongside these efforts, a new approach for improvement of galvanic performance of aluminum sacrificial anodes has been proposed, which showed that the addition of some metal oxides could relatively improve the targeted electrochemical properties. Table 1 shows briefly the major published results for aluminum anodes activation by metal oxide incorporation.

The present research investigates the effect of incorporation of low-cost manganese dioxide concentrate, mainly composed of MnO<sub>2</sub> and SiO<sub>2</sub>, on activation of Al-5% Zn-0.1% Sn and the effect of heat treatment on its galvanic performance at different concentrations of metal oxides,

aiming to reach a clear understanding of the mechanism by which metal oxides enhance anode performance.

## Materials and methods

### Materials

Base metal for these experiments was commercial pure aluminum alloy AA 1070 (0.182 wt.% Fe, 0.037 wt.% Si, 0.047 wt.% Zn), alloyed with 5% of special high-grade zinc (99.99 wt.%) and ultra-pure tin (99.995 wt.%). The commercially available manganese dioxide concentrate powder were selected as an activation additive and had been supplied by Sinai Manganese Co. Phase identification was done using “PANalytical X’Pert PRO” X-ray diffraction facility. The resulted diffractogram has been quantified by the Rietveld method using “HighScore Plus” software suite, compound analysis, and the X-Ray diffraction pattern which are shown in Fig. 1. An aluminum metal matrix composite (AMMC) master alloy is made by the stir casting process with a substrate composed of Al-5% Zn-0.1% Sn incorporated with metal oxides as activation additive. Metal oxides are ground in a ball mill and sieved for particle size of less than 5 microns.

### Fabrication of anode material

The anode material has been fabricated by firstly production of metal matrix composite (MMC) master alloy with oxide volume fraction ( $V_f$ ) of 10 vol.%, followed by using this master alloy for dilution of 4 different concentrations of metal oxides. Master alloy production has been accomplished by stir casting process as shown in Fig. 2, variable speed motor is connected to rotating rod ending with pitch blade type impeller, and the motor head height could be adjusted to modify location of impeller with respect to molten metal height in a graphite crucible, with continuous molten metal temperature measurement using type K thermocouple.

Although the stir casting process is considered the most economic technique for metal matrix composite manufacturing, it has some complications regarding the required fine tuning of its numerous processing parameters like impeller blade type, impeller angle, impeller position inside the melt, stirring speed, stirring time, additives feeding rate, molten metal temperature, and powder pretreatment [19–21]. An extensive work has been dedicated to optimization of stir casting condition for several powders like B<sub>4</sub>C, SiC, B<sub>4</sub>C/Al<sub>2</sub>O<sub>3</sub>, and graphite in different aluminum alloy substrates [22–26], but these results cannot be generalized to our condition as wettability of the added powder is largely dependent on surface tension of aluminum matrix alloy and shape

**Table 1** Aluminum activation using metal oxides

Alloy	Potential (vs SCE)	Current capacity (A·h·kg <sup>-1</sup> )	Current efficiency	Reference
<b>Al-Zn-IrO<sub>2</sub></b>				
Al-5% Zn-0.0425 mg/cm <sup>2</sup> IrO <sub>2</sub>	-0.99	1566	58.5	[15]
Al-5% Zn-0.085 mg/cm <sup>2</sup> IrO <sub>2</sub>	-1	1991	60	[15]
Al-5% Zn-0.175 mg/cm <sup>2</sup> IrO <sub>2</sub>	-1.005	2068	76.3	[15]
Al-5% Zn-0.35 mg/cm <sup>2</sup> IrO <sub>2</sub>	-1.02	2113	81	[15]
<b>Al-Zn-CeO<sub>2</sub></b>				
Al-5% Zn-0.05% CeO <sub>2</sub>	-0.953	1102.08	38.4	[16]
Al-5% Zn-0.1% CeO <sub>2</sub>	-0.957	1833.93	63.9	[16]
Al-5% Zn-0.2% CeO <sub>2</sub>	-0.961	2255.82	78.6	[16]
Al-5% Zn-0.5% CeO <sub>2</sub>	-0.955	1796.62	62.6	[16]
Al-5% Zn-1% CeO <sub>2</sub>	-0.967	1391.95	48.5	[16]
<b>Al-Zn-RuO<sub>2</sub></b>				
Al-5% Zn-0.175% RuO <sub>2</sub>	-1.025	2455	85	[17]
<b>Al-Zn-ZnO</b>				
Al-5% Zn	-0.983	1678.95	58.5	[4]
Al-5% Zn-0.1% ZnO	-0.983	2238.6	78	[4]
Al-5% Zn-0.25% ZnO	-0.991	2296	80	[4]
Al-5% Zn-0.5% ZnO	-0.996	2382.1	83	[4]
<b>Al-Zn-Al<sub>2</sub>O<sub>3</sub></b>				
Al-5% Zn-0.1% Al <sub>2</sub> O <sub>3</sub>	-0.951	1676.08	58.4	[4]
Al-5% Zn-0.25% Al <sub>2</sub> O <sub>3</sub>	-0.955	1722	60	[4]
Al-5% Zn-0.5% Al <sub>2</sub> O <sub>3</sub>	-0.960	1722	60	[4]
<b>Al-Zn-MnO<sub>2</sub></b>				
Al-5% Zn	-0.93	1678.95	58.5	[18]
Al-5% Zn-0.05% MnO <sub>2</sub>	-0.94	1722	60	[18]
Al-5% Zn-0.1% MnO <sub>2</sub>	-0.945	1750.7	61	[18]
Al-5% Zn-0.2% MnO <sub>2</sub>	-0.948	1808.1	63	[18]
Al-5% Zn-0.5% MnO <sub>2</sub>	-0.97	2296	80	[18]
Al-5% Zn-1% MnO <sub>2</sub>	-0.959	2152.5	75	[18]

of particulate. Several preliminary trials have conducted for optimization of stir casting parameters and resulted in producing the targeted master alloy using processing conditions mentioned in Table 2 [27]. The master alloy is then diluted to four different concentrations of metal oxides as mentioned in Table 3.

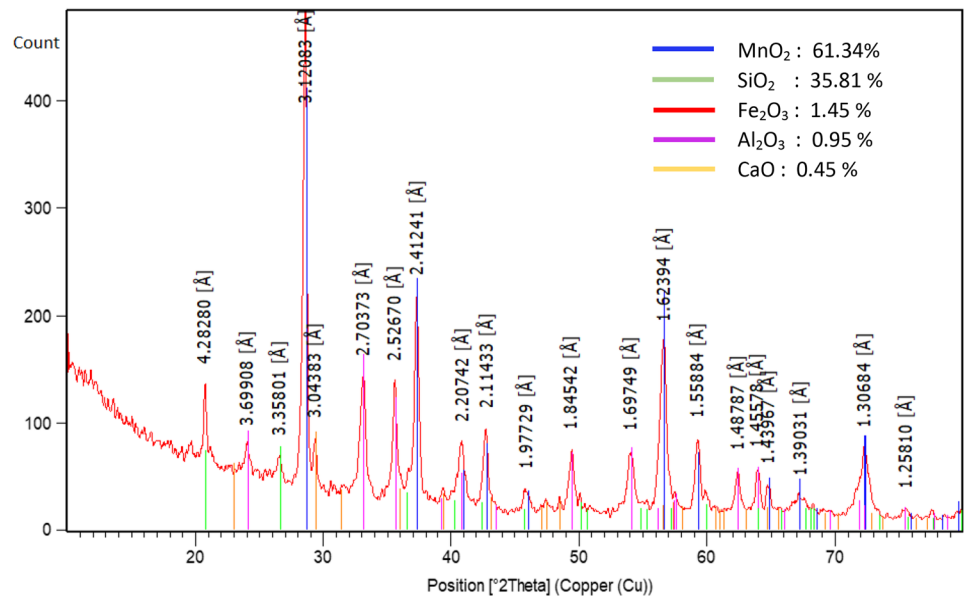
### Heat treatment

To study the effect of heat treatment on galvanic performance of the abovementioned alloys and compare it with the as cast condition, a solution treatment process has been applied to alloys (0, 1, 2, 3 and 4) at three different temperatures (250 °C, 400 °C, 550 °C) for 1 h in a Nabertherm L9/12 muffle furnace, followed by quenching in tap water. Table 4 shows designation of all samples subject to further testing.

### Metallographic analysis

To evaluate the stir casting process for effective incorporation of metal oxides and achieving the required wetting and homogeneity of distribution, microstructure samples have been taken from the investigated alloys and studied using optical microscope (Olympus). The samples for the metallographic examination were ground on grades of SiC emery paper with grit number ranging from P240 to P2000 in sequence using water as a coolant. Fine polishing has been done for samples using 0.5-micron alumina powder on a rotating disc. No etching treatment was applied to avoid revealing intermetallic compounds for proper observation of the added powder. Olympus stream motion software was used to make image quantitative phase analysis to calculate the volume fraction of the added oxides incorporated in the matrix in each case.

**Fig. 1** X-Ray diffraction pattern for metal-oxides mixture used as activation additive



### Evaluation of current efficiency

Evaluation of galvanic performance was done using constant current measurement per DNVGL-RP-B401 [28]. Cylindrical samples machined to a diameter of 10 mm and 50 mm height with a groove for connection are rinsed by tape water followed by ethanol, dried, and weighed. Samples were then coupled with cylindrical mild steel sheet using copper wire and submerged in 10 L of artificial sea water prepared per ASTM D1141 [29]. The composition of mild steel is as follows: 0.064%C, 0.025%Si, 0.2%Mn, 0.017%P, 0.011%S, 0.013%Cr, 0.022% Ni, and Fe balance.

Samples were suspended in the center of the uncoated cylindrical steel sheet, such that the wetted surface area of

steel cathode is at least 25 times the exposed area of anode specimen, the solution is continuously stirred with air bubbling blowers to avoid occurrence of concentration polarization. Testing cells were connected in series with a programmable DC Regulated Power Supply (DPS3005D, output 0–30 V and 0–5 A, 10 mV/1 mA high accuracy and resolution) for galvanostatic control; the specimen and the cathode were coupled to the positive and negative rectifier terminals, respectively as shown in Fig. 3.

For measurement of the total discharged current, two copper coulometers were inserted in series with the circuit for current integration with an accuracy of  $\pm 2\%$ . Copper coulometer were built per NACE TM-0190 [30], each coulometer mainly consisted of two copper plates connected with positive

**Fig. 2** Schematic of stir casting equipment

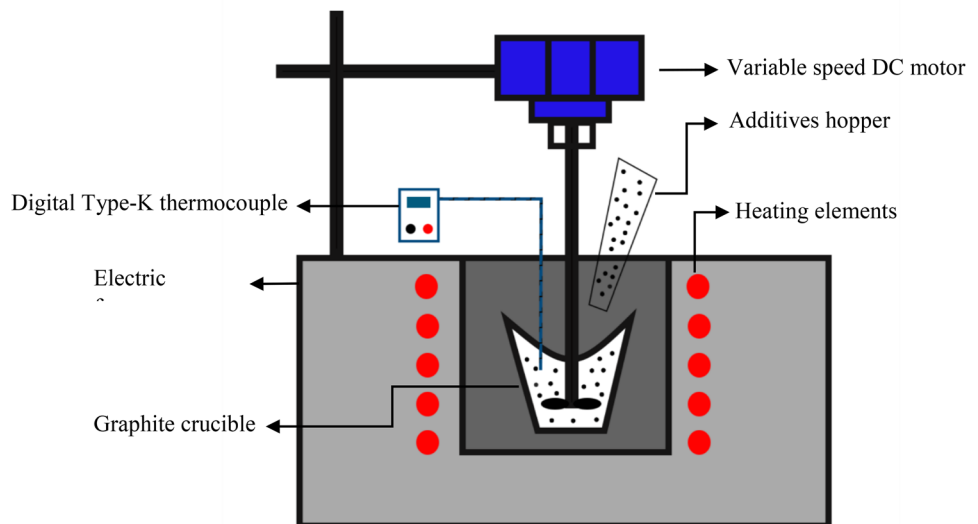


**Table 2** Optimized processing conditions for stir casting [27]

Processing parameters	
Stirring speed	700 rpm
Stirring time	5 min
Feeding rate	10 g/min
Blade location inside the melt	Below 0.3 of melt height
Stirring blade type	Pitch blade type
Stirring blade angle	60 degrees
Start melt temperature	720 °C
Finish melt temperature	640 °C

terminal and a central copper winning wire connected to the negative terminal all submerged in CuSO<sub>4</sub> electrolyte (100 g/L CuSO<sub>4</sub>, 25 mL/L H<sub>2</sub>SO<sub>4</sub>, 25 mL/L ethanol) [31]. The test is run for four continuous days with varying current density as 1.5, 0.4, 4, and 1.5 mA/cm<sup>2</sup> for days 1 to 4 respectively. At the end of the test, samples were cleaned from corrosion products by immersion in a solution of 41 mL H<sub>3</sub>PO<sub>4</sub>+28 g Cr<sub>2</sub>O<sub>3</sub>+1.4 l water at 80 °C for about 5 min. Then, the samples were dried and weighed again.

For calculation of the actual current capacity of the aluminum anodes, we use the weight of copper deposits on the copper coulometer wire to measure the total amount of charge transferred throughout the circuit during the test using Faraday's Law of electrolysis Eq. (1). Dividing the total charge transferred by the weight loss of each aluminum anode will result the actual current capacity for each anode. These calculations are formulated in a simplified form in NACE TM-0190 as expressed in Eqs. (2)–(3).

$$\text{Faraday's law } m = \frac{MQ}{nF} \quad (1)$$

$$\text{Actual Current Capacity (A.h/kg)} = \frac{0.8433 \times W_{cu}}{W_{al}} \times 1000 \quad (2)$$

$$\text{Current Efficiency} = \frac{\text{Actual current capacity}}{\text{Theoretical current capacity}} \quad (3)$$

**Table 3** Nominal alloy compositions

Alloy	Metal oxides (vol.%)	Zn (wt.%)	Sn (wt.%)	Al (wt.%)
Reference (alloy 0)	-	5	0.1	Remainder
Master alloy	10.62	5	0.1	Remainder
Alloy 1	1.7	5	0.1	Remainder
Alloy 2	3.8	5	0.1	Remainder
Alloy 3	5.6	5	0.1	Remainder
Alloy 4	8.2	5	0.1	Remainder

**Table 4** Samples designation

Alloy composition	Al-5Zn-0.1Sn				
	0%	1.70%	3.8 0%	5.60%	8.20%
Metal oxides V <sub>f</sub>					
As Cast	0-AC	1-AC	2-AC	3-AC	4-AC
Solution treated at 250 °C	0-1	1-1	2-1	3-1	4-1
Solution treated at 400 °C	0-2	1-2	2-2	3-2	4-2
Solution treated at 550 °C	0-3	1-3	2-3	3-3	4-3

where  $m$  is the deposited/liberated mass of material at the electrode after electrolysis (in grams),  $M$  is the molecular weight of the element (in g/mol),  $Q$  is the total charge transfer in coulomb (A sec),  $n$  is the number of valence electrons transferred during ionization which is 3 and 2 for Al and Cu respectively, and  $F$  is the Faraday constant 96,485 C/mol.  $W_{cu}$  is mass gained by copper cathode wire of coulometer after the end of the test and  $W_{al}$  is mass loss of anode samples both measured in grams. Knowing that theoretical current capacity of Al-5Zn is 2870 A h/kg calculated using Faraday's law.

Alongside with samples mentioned in Table 5, a commercial Galvalum III sample (Al-0.16% In-3.5% Zn) has been test for comparison.

### OCP and CCP measurement [28]

The open circuit potential (OCP), the potential difference between the test anodes with respect to standard calomel electrode (SCE), was measured for each sample after stabilizing for 15 min in 3% NaCl solution at 30 ± 2 °C. The closed circuit potential (CCP) of the test anodes was measured at the end of 4-day galvanostatic coupling with mild steel cathodes. CCP was taken as the average of three measurements per specimen at different positions using a SCE with an electrolyte bridge such that the tip of the bridge was positioned within 1 mm from the specimen surface without disturbing any corrosion products formed over the specimen.

### Potentiodynamic polarization

One square centimeter sample coupons have been prepared according to ASTM G59 [32], samples are polished against emery paper at different grades up to P1200, and then samples were tested using potentiostat–galvanostat (Versa Stat) after 15 min of stabilization at rest potential. After stabilization, polarization has been done at a scan rate of 0.01 V/s. Testing coupons were connected as working electrode against platinum electrode and SCE as counter electrode and reference electrode respectively.

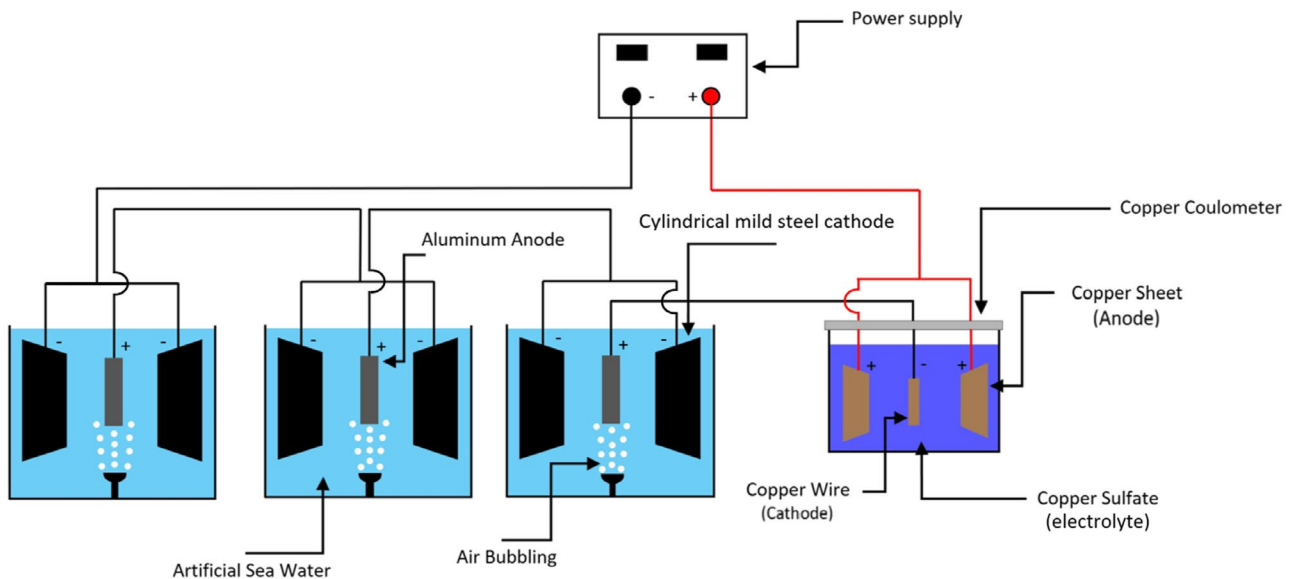


**Fig. 3** Schematic of galvanic test cells of sacrificial anodes

### Scanning electron microscope analysis

After the end of the galvanic performance test, slices from test anodes have been cut for in-depth characterization of dissolution behavior. Samples are metallographically

**Table 5** Galvanic performance results of Al-5Zn-0.1Sn incorporated with different concentrations of metal oxides at different heat treatments

Samples	OCP (V)	CCP after 96 h (V)	Current capacity (A h/kg)	Current efficiency (%)
0-AC	-1.080	-0.943	2062.96	71.88
0-1	-1.062	-0.945	1705.35	59.42
0-2	-1.089	-0.942	1474.89	51.39
0-3	-1.050	-0.947	2287.10	79.69
1-AC	-1.073	-0.950	2156.52	75.14
1-1	-1.068	-0.945	1858.32	64.75
1-2	-1.091	-0.946	1578.21	54.99
1-3	-1.073	-0.950	2408.50	83.92
2-AC	-1.038	-0.955	2323.55	80.96
2-1	-1.035	-0.940	1971.12	68.68
2-2	-1.098	-0.948	1735.78	60.48
2-3	-1.075	-0.942	2518.14	87.74
3-AC	-1.028	-0.944	2360.86	82.26
3-1	-1.063	-0.949	1791.74	62.43
3-2	-1.020	-0.942	1711.38	59.63
3-3	-1.090	-0.946	2678.86	<b>93.34</b>
4-AC	-1.011	-0.955	2226.83	77.59
4-1	-1.000	-0.955	1813.55	63.19
4-2	-1.059	-0.940	1653.98	57.63
4-3	-1.072	-0.948	2542.82	88.60
Galvalum III	-1.091	-0.954	2357.00	81.20

prepared and examined using scanning electron microscope (Bruker); investigation has been done to corrosion interface of anode and its bulk non-reacted core using secondary electron imaging, energy dispersive x-ray analysis (EDX), and elemental mapping.

## Results and discussion

### Microstructure evaluation of stir casting process

Adoption of process parameters mentioned in Table 4 resulted fairly homogenous distribution of metal oxides after dilution of master alloy as shown in Fig. 4. We observed that at low stirring speed (300 rpm) vortex was not strong enough to withdraw and trap the powder inside the melt; however, at very high stirring speed (1100 rpm), a very strong vortex is formed which resulted in noticeably high air suction resulting in higher oxidation rate and very high losses in form of dross reaching 40% of melt weight. The optimum stirring speed was found to be 700 rpm. Another critical factor for effective incorporation of the investigated oxides is the powder feeding rate; high feeding rate did not give enough chance for powder to enter the vortex and caused stoppage of the aimed vortex shape.

### Evaluation of galvanic performance

The current capacity and current efficiency of all samples are shown in Table 5 and graphically represented in Fig. 5. From which we can notice, addition of metal oxides has improved



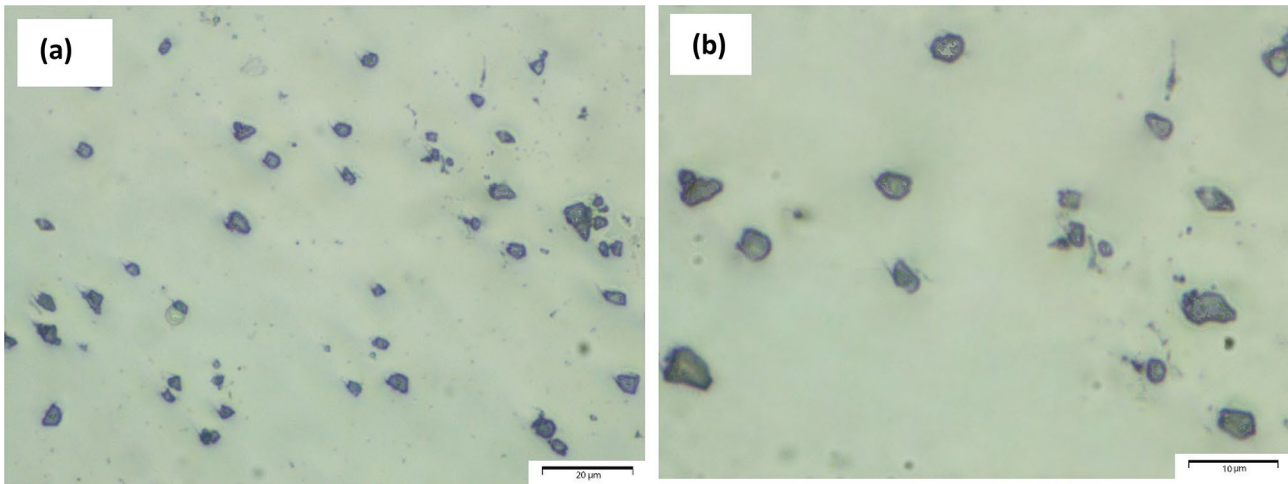


**Fig. 4** Microstructure images of alloy 4 showing decent distribution of metal oxides and fair degree of wetting with the matrix **a** at 1000 $\times$  and **b** at 2000 $\times$

galvanic efficiency of anodes in the as cast condition from 71.88 to 82.26% at 5.6 vol.% of metal oxides. The effect of solution treatment of samples at 550 °C is most recognizable in improvement of galvanic performance in all cast compositions, but this effect is more obvious for 5.6 vol.% of metal oxides with efficiency of 93.24% compared with 79.69% for alloy without metal oxides incorporation. However, solution treatments at 250 °C and 400 °C are found to be detrimental to current efficiency in all alloy compositions. Interpretation of these results is more understood from the SEM images investigation in the upcoming section.

In comparison with the tested Galvalum III sample, sample 3–3 solution treated at 550 °C give superior performance over the commercial alloy with around 15% improvement in current capacity.

For observation of corrosion surface morphology, Fig. 6 shows the surface corrosion features of all tested samples. The macro-attack morphology for samples solution treated at 250 °C and 400 °C shows severe grain separation which resulted in serious self-corrosion giving poor electrochemical properties. Samples solution treated at 550 °C show uniform pitting attack in different severities for anode

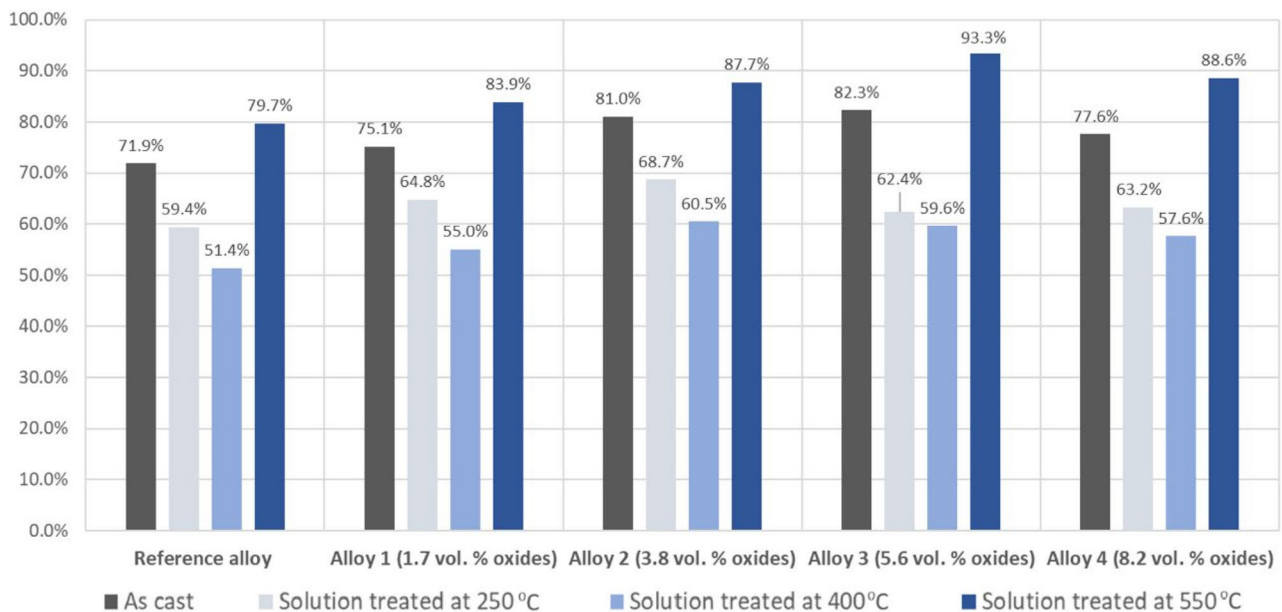
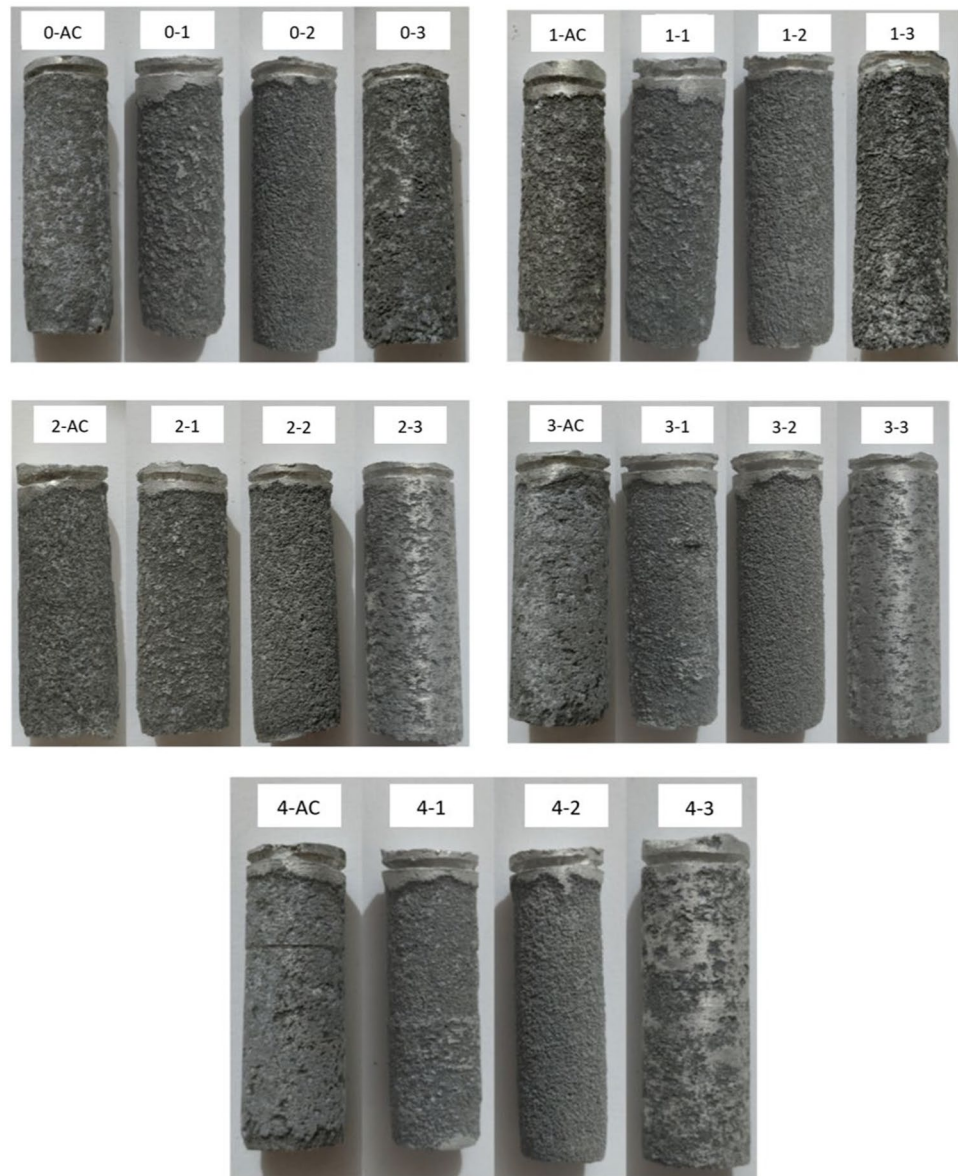


**Fig. 5** Bar chart for galvanic performance of tested samples

**Fig. 6** Surface corrosion features of all samples tested



composition with no indications for particle shedding from anode surface during testing which explains the high current efficiency of these samples. However, as cast samples show uniform corrosion with moderate grain separation giving intermediate galvanic performance.

Regarding the electrode potentials in Table 5, OCP with a range of  $-1.00$  to  $-1.098$  V has been observed when samples are measured against SCE. After coupling for 96 h during the galvanic performance test, potential has increased due to formation of corrosion products over the anode surface and generated some kind of resistance for ion transfer. CCP has been reported with a very narrow range of potential ( $-0.94$  V to  $-0.955$  V) versus SCE, these small differences in millivolts are not believed to

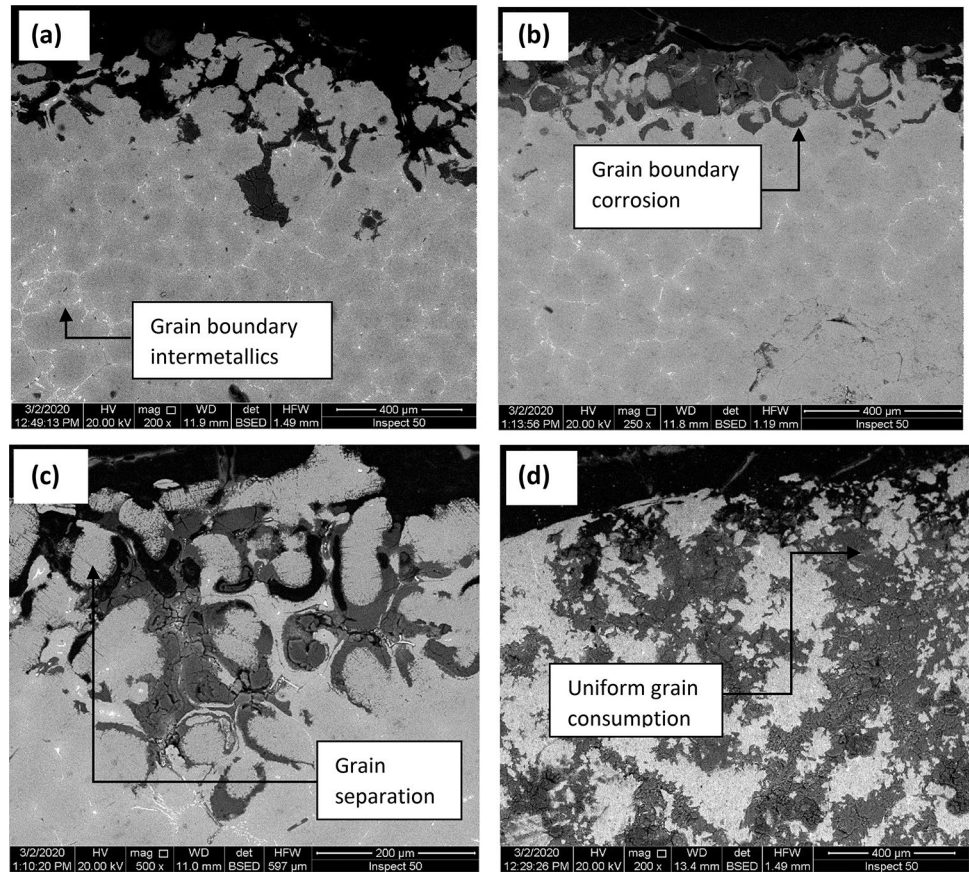
reflect a major distinction between samples in terms of anodic activity. However, these values of CCP satisfy the cathodic protection criteria for corrosion stoppage of steel components which is  $-850$  mV SCE. Additionally, this range of CCP comfortably lies in the optimum potential for cathodic potential which is  $-0.850$  to  $-0.995$  V versus SCE without showing any degree of over protection [33].

### Scanning electron microscope analysis

SEM imaging and EDX elemental mapping could give a clear explanation for characteristic results of galvanic performance tests. SEM analysis in Fig. 7 reveals the presence of two distinct modes of corrosion, namely the localized inter



**Fig. 7** Scanning electron microscope images for specimens' corrosion interface after completion of galvanic performance test **a** sample 0-AC, **b** sample 3-1, **c** sample 3-2, **d** sample 2-3



granular surface corrosion, in the as cast specimens and in the low temperatures heat treated samples, and the general in-depth corrosion after solution heat treatment at relatively higher temperature.

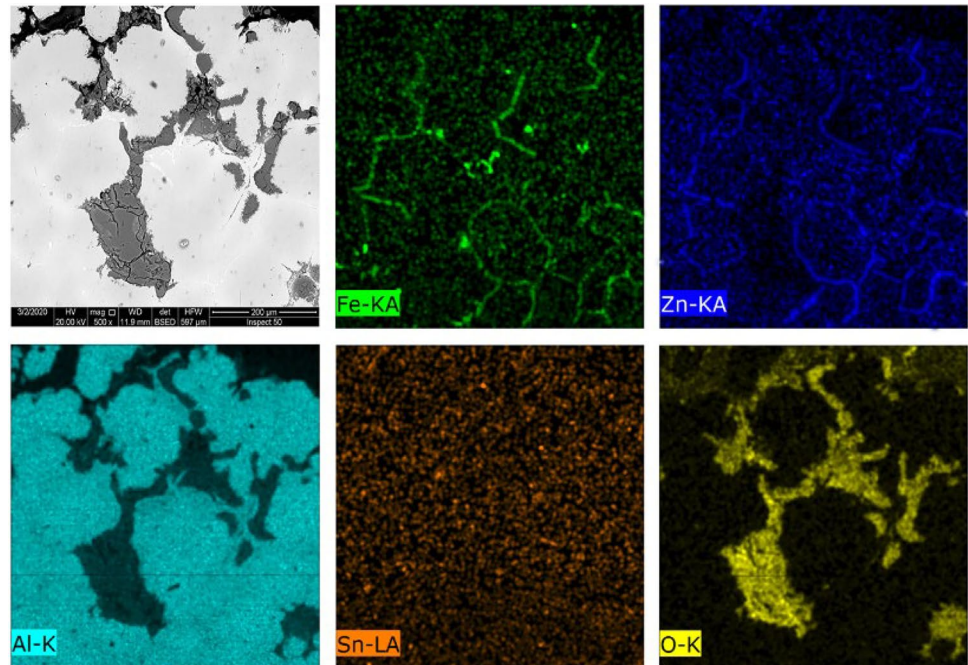
The as cast specimens 0-AC in Fig. 7a reveal the presence of network precipitates at the grain boundaries, which could be responsible for the grain disintegrations at the specimen surface. The solution treated samples 3-1 and 3-2, as given in Fig. 7b and c respectively, also showed drastic grain separation and shedding of bulk anode material without being electrochemically consumed in anodic reaction. Conversely, samples solution treated at 550 °C, as given in Fig. 7d, showed uniform corrosion throughout depth of samples giving the opportunity for the whole grain to corrode and give its current capacity for electrochemical reaction.

EDX elemental mapping for 0-AC sample in Fig. 8 shows formation of Fe-Zn intermetallics at grain boundaries which causes formation of micro-galvanic cells between grains and grain boundaries; this localized corrosion is the responsible mechanism for activation as showed by Barbucci et al. [34]. Figure 9 shows that heat treatment at 400 °C triggered segregation of iron and zinc to grain boundaries which caused serious self-corrosion, and parts of the matrix fell off from

surface of the alloy, resulting in the “metallic sponge” feature of its surface morphology and the lower current efficiency [35]. However, the solution treated sample at 550 °C show noticeable dissolution and better distribution of intermetallics, which decreased the localized attack on grain boundaries and explained the increase of anodes current efficiency as shown in Fig. 10 [36].

The effect of activating additives and their interaction with aluminum matrix is more intricate; by studying the behavior of the two main oxides incorporated ( $\text{MnO}_2$  and  $\text{SiO}_2$ ), we can notice that manganese dioxide has undergone an in situ metallothermic reduction by aluminum during master alloy processing and master alloy dilution as aluminum has much higher affinity for formation of stable oxide than manganese [37, 38]. This resulted in reduction of Mn into the matrix as shown by its homogeneous distribution in EDX elemental mapping Figs. 8 and 9. This result is not matching with observations of Shibli et al. that showed retention of  $\text{MnO}_2$  particles after melting [18–39]. The reduced manganese is not observed to have a remarkable contribution to the micro-galvanic corrosion cells and its rule could be limited to disruption of the ionic structure of aluminum passive oxide layer which is

**Fig. 8** EDX elemental mapping of corrosion interface for sample 0-AC



the same effect known for tin or by introducing intermetallic compound ( $\text{Al}_{12}\text{Mn}$ ) with relatively different potential from that of the matrix [7, 10]. However, incorporation of

silica is thought to have a major role in activation process. Silica is not reduced as easily as  $\text{MnO}_2$  by aluminum as it needs a temperature of around 1200 °C and holding time

**Fig. 9** EDX elemental mapping of corrosion interface for sample 3–2

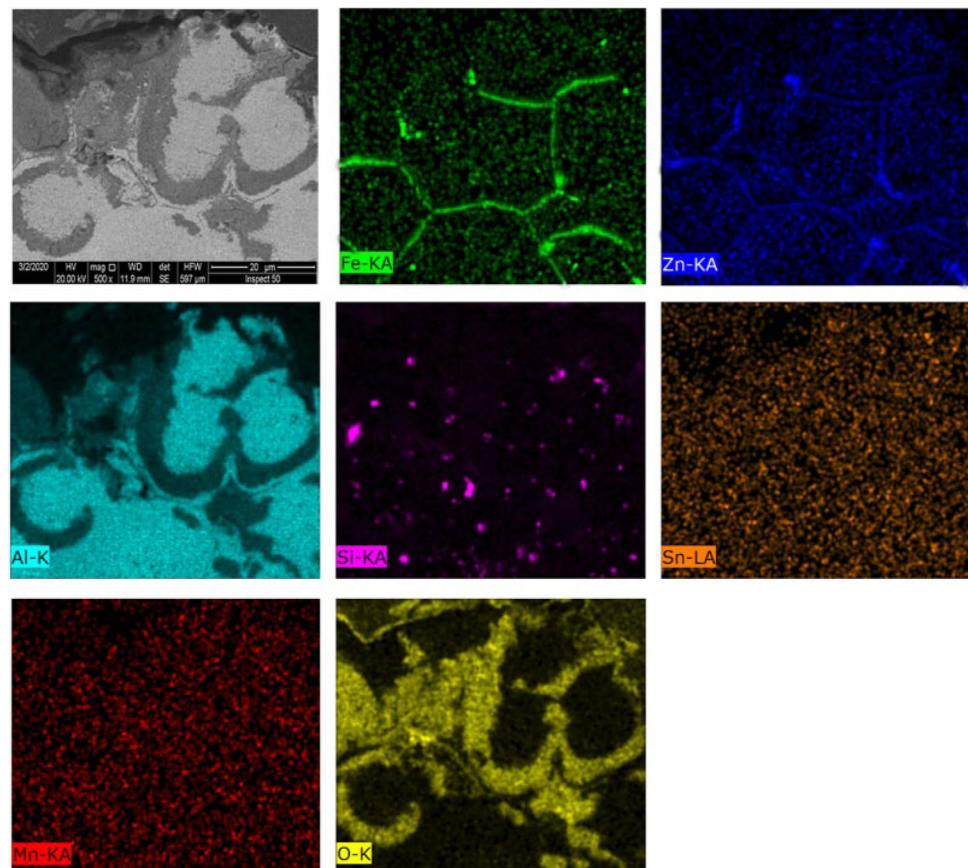
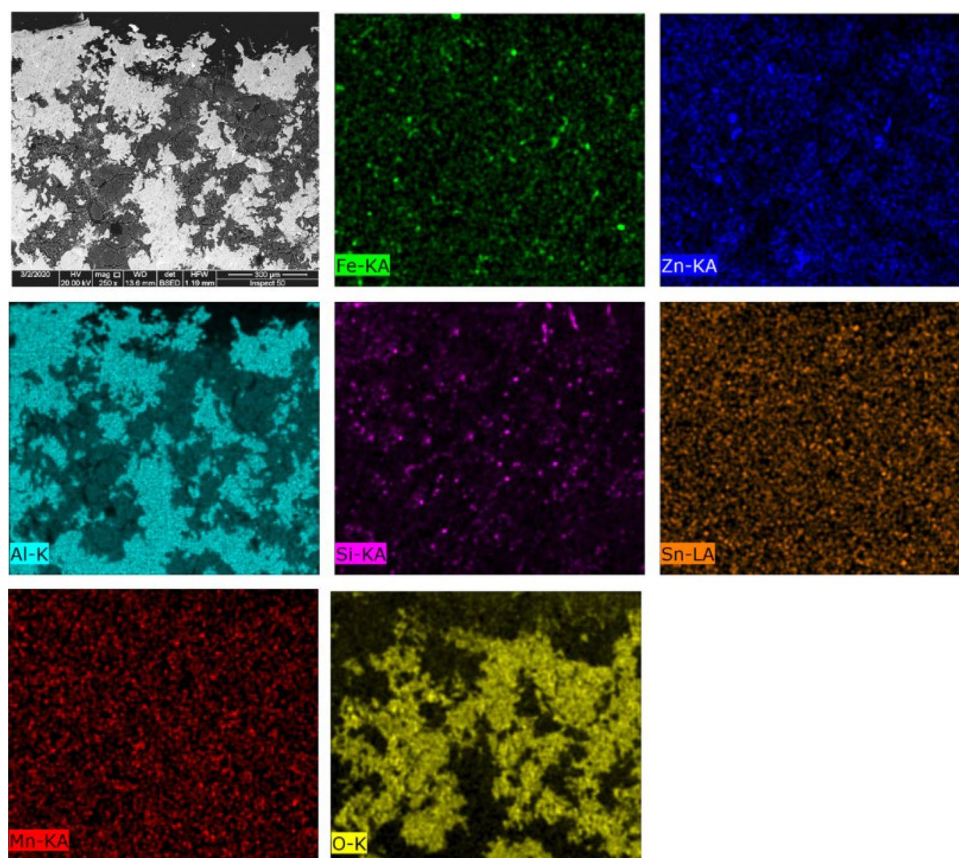




**Fig. 10** EDX elemental mapping of corrosion interface for sample 3–3



of 30–120 min to complete the reduction [40]; these conditions of superheating and mixing time are not provided by manufacturing process in this work. Nonetheless, Afsaneh et al. [41] showed that an interfacial reaction could take place between aluminum and the impeded silica particles at much lower temperatures forming an interphase between silica particles and the matrix.  $\text{SiO}_2$  causes interruption in oxide film layer of aluminum giving the chance to electrolyte in interact with bulk aluminum grains. Additionally, SEM image in Fig. 11 shows the effect of incorporated  $\text{SiO}_2$  particles which act as initiation points for additional microgalvanic cells with the matrix inside the bulk grains making corrosion more distributed over the whole-grain structure instead of being localized at grain boundaries. This effect is believed to be behind the improvement of current efficiency up to 93% for samples incorporated with activating oxides and heat treated at 550 °C by giving more potential for anode material to be electrochemically consumed in the anodic reaction and give useful protection current instead of grain loss which is associated with the high self-corrosion rate other samples.

### Polarization curves

The effect of metal oxide incorporation at different heat treatments on potentiodynamic polarization behavior is shown in Fig. 12. Tafel curves manifest some characteristic features for samples' behavior as sacrificial anodes. We noticed that samples solution treated at 250 °C and 400 °C show a lower  $E_{\text{corr}}$  compared with samples treated at 550 °C, the lower  $E_{\text{corr}}$  generally means more efficient surface activation. However, this higher activation was accompanied with relatively higher corrosion rates as shown in the summarized polarization data in Table 6. The decrease in  $i_{\text{corr}}$  for samples treated at 550 °C is in good agreement with its relatively lower corrosion rate, which refers to the positive effect in minimizing non-coulombic losses. Studying a pure aluminum sample, we notice that pure Al exhibits a wide passivation region which is represented by a plateau in current density, having this polarization resistance is the reason behind non-suitability of pure aluminum for cathodic protection.

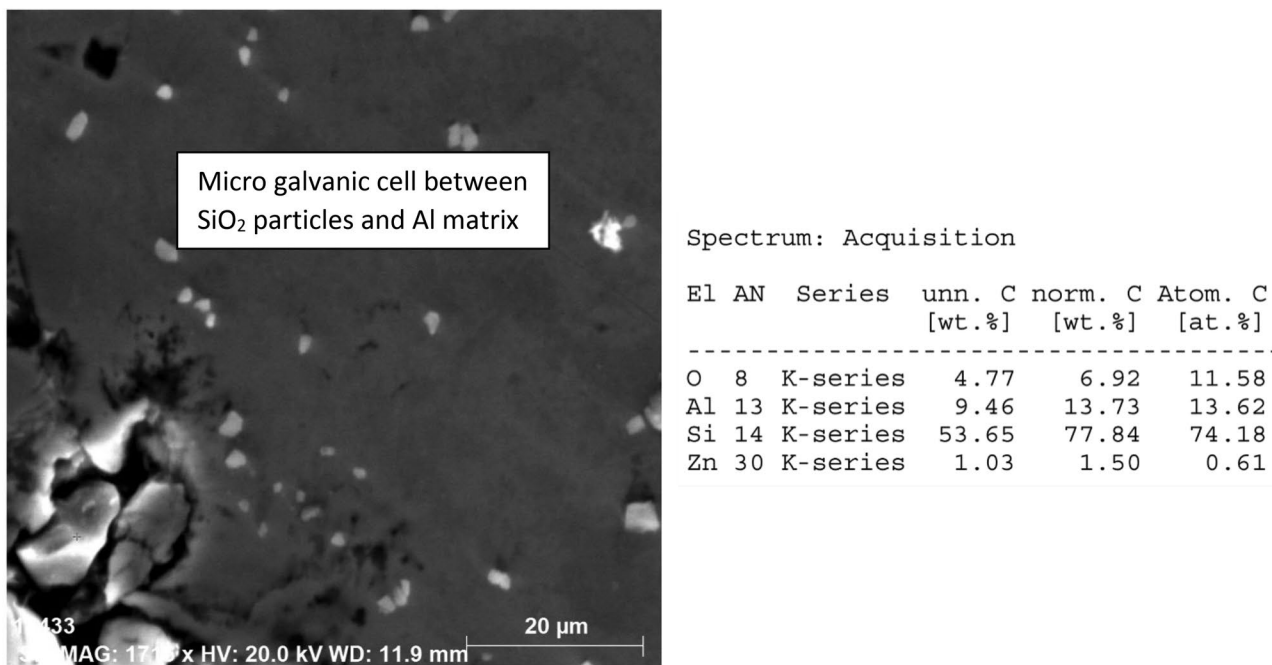


Fig. 11 Interaction between SiO<sub>2</sub> particles and anode matrix shows formation of micro-galvanic cell within the grain

On the other hand, the effect of activators added to the modified alloys shows dramatic decrease in the passivation plateau which indicates to the efficient breakdown of passive oxide layer. We can also notice that all samples

that gave higher current efficiency are showing relatively higher pitting potential over samples exhibiting grain separation and lower current efficiency, which can correlate galvanic performance with surface corrosion morphology.

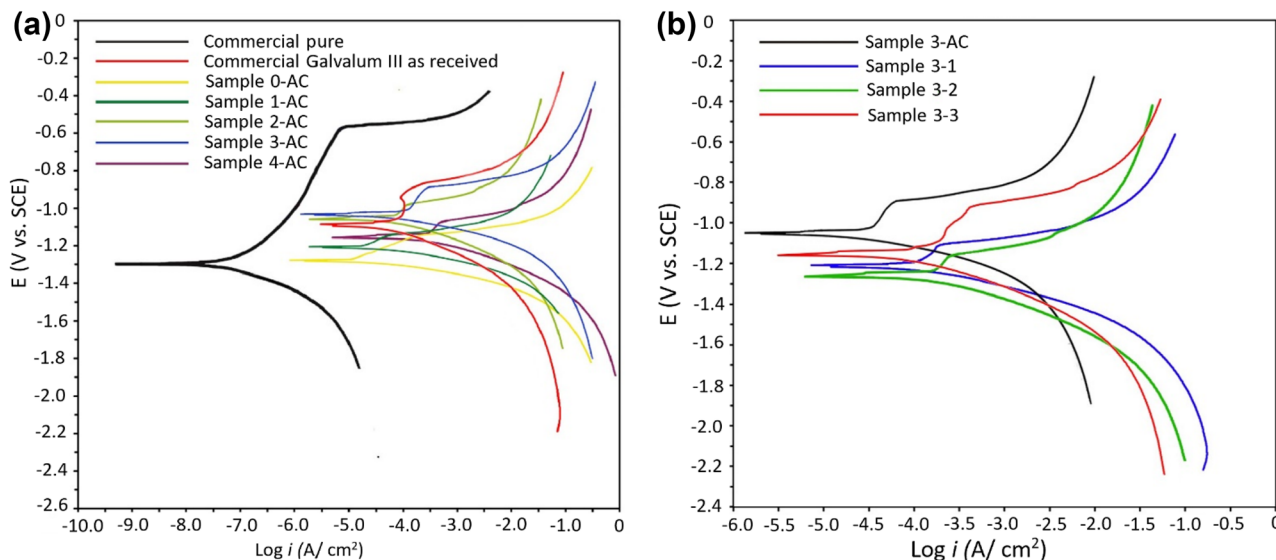


Fig. 12 Potentiodynamic polarization curves **a** polarization curves of as cast samples compared with pure aluminum and commercial Galvalum III, **b** polarization curves of the optimum condition of alloy 3 with 5.6 vol.% of oxides

**Table 6** Potentiodynamic test results all as cast samples, samples for optimum metal oxides volume fraction (5.6%), and for commercial pure aluminum and as received Galvalum III as for comparison

Sample	I corr (micro A)	Corrosion rate (mm/year)	E corr (V)	$\beta_a$ (V/dec)	$-\beta_a$ (V/dec)	$R_p$ ( $\Omega \text{ cm}^2$ )
A1070 aluminum	0.32	0.003	− 1.310	0.544	0.210	208,437.4
Galvalum	46.77	0.510	− 1.090	0.173	0.051	366.9
<b>As cast samples</b>						
0-AC	10.47	0.114	− 1.290	0.113	0.030	995.6
1-AC	16.22	0.177	− 1.210	0.119	0.023	517.0
2-AC	64.56	0.704	− 1.070	0.276	0.101	498.9
<b>3-AC</b>	120.23	1.311	− 1.040	0.442	0.059	188.7
4-AC	281.84	3.074	− 1.160	0.380	0.096	118.2
<b>Optimum composition</b>						
3–1	112.20	1.224	− 1.210	0.504	0.099	320.2
3–2	138.04	1.506	− 1.270	0.433	0.133	320.3
<b>3–3</b>	70.79	0.772	− 1.160	0.332	0.169	686.4

## Conclusion

On the basis of the investigation of Al-5Zn-0.1Sn alloy incorporated with activating additives ( $\text{SiO}_2$  and  $\text{MnO}_2$ ) and solution treated at different temperatures, the following conclusions can be drawn:

1. Incorporation of  $\text{SiO}_2$  has shown an improvement in galvanic performance properties that is presumed to occur due to initiation of additional micro-galvanic cells inside the grains—other than grain boundaries—which makes corrosion more uniform inside anode bulk material instead of being localized on grain boundaries.
2. Incorporation of  $\text{MnO}_2$  is not believed to have significant effect as a metal oxide on galvanic properties of Al sacrificial anodes as it has undergone an aluminothermic reduction reaction leading to dissolution into anode material. However, Mn could influence anode performance through another mechanism, either by modification of ionic structure of  $\text{Al}_2\text{O}_3$  oxide layer or by introducing intermetallic compound ( $\text{Al}_{12}\text{Mn}$ ) with potential different from that of the matrix
3. Solution treatment of anodes also affected anodes' performance; solution treatment at 250 °C and 400 °C has led to acceleration of atomic diffusion and segregation of alloying elements on grain boundaries leading to more intermetallics accompanied with more severe localized corrosion and grain shedding.
4. Solution treatment at 550 °C was high enough for dissolution of major intermetallics, which led to more uniform corrosion spread throughout anode material without noticeable grain separation.

**Acknowledgements** The authors are grateful to the staff of the pilot casting unit Central Metallurgical Research and Development Institute (CMRDI) for dedicating their time and effort to facilitate this research work.

**Funding** Open access funding provided by The Science, Technology & Innovation Funding Authority (STDF) in cooperation with The Egyptian Knowledge Bank (EKB).

## Declarations

**Conflict of interest** The authors declare no competing interests.

**Open Access** This article is licensed under a Creative Commons Attribution 4.0 International License, which permits use, sharing, adaptation, distribution and reproduction in any medium or format, as long as you give appropriate credit to the original author(s) and the source, provide a link to the Creative Commons licence, and indicate if changes were made. The images or other third party material in this article are included in the article's Creative Commons licence, unless indicated otherwise in a credit line to the material. If material is not included in the article's Creative Commons licence and your intended use is not permitted by statutory regulation or exceeds the permitted use, you will need to obtain permission directly from the copyright holder. To view a copy of this licence, visit <http://creativecommons.org/licenses/by/4.0/>.

## References

1. Chen X, Li XG, Du CW, Cheng YF (2009) Effect of cathodic protection on corrosion of pipeline steel under disbonded coating. *Corros Sci* 51(9):2242–2245. <https://doi.org/10.1016/j.corsci.2009.05.027>
2. Zhang T, Zhao W, Li T, Zhao Y, Deng Q, Wang Y (2017) Comparison of hydrogen embrittlement susceptibility of three cathodic protected subsea pipeline steels from a point of view of hydrogen permeation. *Corros Sci* 1. <https://doi.org/10.1016/j.corsci.2017.11.013>
3. Cicek V (2013) Cathodic protection: industrial solutions for protecting against corrosion. Wiley



4. Shibli SMA, Jabeera B, Manu R (2007) Development of high performance aluminium alloy sacrificial anodes reinforced with metal oxides. *Mater Lett* 61(14–15):3000–3004. <https://doi.org/10.1016/j.matlet.2006.10.062>
5. El Shayeb HA, El Wahab FMA, El Abedin SZ (2001) Electrochemical behaviour of Al, Al-Sn, Al-Zn and Al-Zn-Sn alloys in chloride solutions containing stannous ions. *Corros Sci* 43
6. Shrieber CF, Reding JJ (1967) Field testing a new aluminum anode: AL-Hg-Zn galvanic anode for seawater applications. *Mater Prot* 6:33–36
7. Perkins J, Cummings JR, Reinhardt RA, Graham KJ (1978) Corrosion behavior of aluminum alloys intended for sacrificial anode application in seawater. *Nav Postgrad Sch* 3
8. Bessone JB (2006) The activation of aluminium by mercury ions in non-aggressive media. *Corros Sci* 48(12):4243–4256. <https://doi.org/10.1016/j.corsci.2006.03.013>
9. Reboul MC, Delatte MC (1980) Activation mechanism for sacrificial Al-Zn-Hg anodes. *Mater Perform* 19(5):35–40
10. Lemieux E, Hartt W, Lucas K (2001) A critical review of aluminum anode activation, dissolution mechanisms, and performance. *NACE Int*. NACE-01509
11. Tan J, Nisancioglu K (2013) Effect of small amounts of alloyed tin on the electrochemical behaviour of aluminium in sodium chloride solution. *Corros Sci* 76:219–230. <https://doi.org/10.1016/j.corsci.2013.06.045>
12. Perkins J, Cummings JR, Reinhardt RA, Graham KJ (1978) Corrosion behavior of aluminum alloys intended for sacrificial anode application in seawater. *Nav Postgrad Sch*
13. Newport JT, Reding JJ (1966) The influence of alloying elements on aluminum anodes in seawater. *Mater Prot* 16(2)
14. Snith SN, Reding JT, Riley RL (1976) Development of a broad application saline water aluminum anode – “Galvalum” III
15. Shibli SMA, Gireesh VS (2003) Surface activation of aluminium alloy sacrificial anodes by IrO<sub>2</sub>. *Appl Surf Sci* 219(3–4):203–210. [https://doi.org/10.1016/S0169-4332\(03\)00675-5](https://doi.org/10.1016/S0169-4332(03)00675-5)
16. Shibli SMA, Archana SR, Muhamed Ashraf P (2008) Development of nano cerium oxide incorporated aluminium alloy sacrificial anode for marine applications. *Corros Sci* 50(8):2232–2238. <https://doi.org/10.1016/j.corsci.2008.06.017>
17. Shibli SMA, George S (2007) Electrochemical impedance spectroscopic analysis of activation of Al-Zn alloy sacrificial anode by RuO<sub>2</sub> catalytic coating. *Appl Surf Sci* 253(18):7510–7515. <https://doi.org/10.1016/j.apsusc.2007.03.052>
18. Shibli SMA, Binoj KK (2009) Development of MnO<sub>2</sub>-incorporated high performance aluminum alloy matrix sacrificial anodes. *J Appl Electrochem* 39(2):159–166. <https://doi.org/10.1007/s10800-008-9659-3>
19. Hashim J, Looney L, Hashmi MSJ (2002) Particle distribution in cast metal matrix composites-Part I. *J Mater Process Technol* 123(2):251–257. [https://doi.org/10.1016/S0924-0136\(02\)00098-5](https://doi.org/10.1016/S0924-0136(02)00098-5)
20. Hashim J, Looney L, Hashmi MSJ (2002) Particle distribution in cast metal matrix composites- Part II. *Mater Process Technol* 123(2):258–263. [https://doi.org/10.1016/S0924-0136\(02\)00099-7](https://doi.org/10.1016/S0924-0136(02)00099-7)
21. Annigeri UK, Veeresh GB (2017) Method of stir casting of aluminum metal matrix composites: a review. *Mater Today Proc* 4(2):1140–1146. <https://doi.org/10.1016/j.matpr.2017.01.130>
22. Ramnath BV, Elanchezhian C, Jaivignesh M, Rajesh S, Parswajinan C, Ahmed AS (2014) Evaluation of mechanical properties of aluminium alloy – alumina – boron carbide metal matrix composites. *J Mater* 58:332–338. <https://doi.org/10.1016/j.matdes.2014.01.068>
23. Pozdniakov AV, Zolotorevskiy VS, Barkov RY, Lotfy A, Bazlov AI (2016) Microstructure and material characterization of 6063/B<sub>4</sub>C and 1545K/B<sub>4</sub>C composites produced by two stir casting techniques for nuclear applications. *J Alloys Compd* 664:317–320. <https://doi.org/10.1016/j.jallcom.2015.12.228>
24. Balasivanandha Prabu S, Karunamoorthy L, Kathiresan S, Mohan B (2006) Influence of stirring speed and stirring time on distribution of particles in cast metal matrix composite, *J Mater Process Technol* 171(2):268–273. <https://doi.org/10.1016/j.jmatprotec.2005.06.071>
25. Baradeswaran A, Perumal AE (2014) Wear and mechanical characteristics of Al 7075/graphite composites. *Compos Part B Eng* 56:472–476. <https://doi.org/10.1016/j.compositesb.2013.08.073>
26. Reza H, Abolkarim S, Haddad M, Huang Y (2014) “Investigation of microstructure and mechanical properties of Al6061-nanocomposite fabricated by stir casting. *J Mater* 55:921–928. <https://doi.org/10.1016/j.matdes.2013.10.060>
27. Abdelrahman A, Nofal A, Attia G (2020) Optimization of stir casting process parameters for producing MMC aluminum sacrificial anode incorporated with manganese dioxide concentrate powder. *Int J Eng Res Technol* 13(10):2651–2659. <https://doi.org/10.37624/IJERT/13.10.2020.2651-2659>
28. Det Norske Veritas, Cathodic protection design, DNV-RP-B401.
29. ASTM D1141–98 (2013) Standard practice for the preparation of a substitute ocean water. ASTM International, West Conshohocken, PA
30. NACE International Store (2012) TM0190–2012 impressed current laboratory testing of aluminum alloy anodes, Texas
31. Haque I, Khan A, Rasheed A (2006) Cathodic efficiency of industrial chromium plating. *Pak J Sci Ind Res* 49(3):222–224
32. ASTM G59–97 (2014) Standard test method for conducting potentiodynamic polarization resistance measurements Am Soc Test Mater. DOI:<https://doi.org/10.1520/g0059>.
33. Gurrappa I (2005) Cathodic protection of cooling water systems and selection of appropriate materials. *J Mater Process Technol* 166(2):256–267. <https://doi.org/10.1016/j.jmatprotec.2004.09.074>
34. Barbucci A, Cerisola G, Bruzzone G, Saccone A (1997) Activation of aluminium anodes by the presence of intermetallic compounds. *Electrochim Acta* 42(15):2369–2380. [https://doi.org/10.1016/S0013-4686\(96\)00420-3](https://doi.org/10.1016/S0013-4686(96)00420-3)
35. Zhu C, Xu F, Wei W, Ding Y, Wang N (2005) Effect of Sb and Sn on performance of aluminum sacrificial anode materials. *Chinese J Nonferrous Met* 15(4):631–636
36. Salinas D, Bessone J (1991) Electrochemical behavior of Al-5%Zn-0.1%Sn sacrificial anode in aggressive media: influence of its alloying elements and the solidification structure. *Corrosion* 47(9):665–674
37. Jiaying S, Tao G, Wen D, Yiming M, Xiang F, Hao W (2018) Study on thermal chemical reaction of Al/MnO<sub>2</sub> thermite, *IOP Conf. Ser.: Earth Environ Sci* 186(2). <https://doi.org/10.1088/1755-1315/186/2/012046>.
38. Sarang B, Sarang A, Ray HS (1996) Kinetics of aluminothermic moanalytical investigation reduction of MnO<sub>2</sub> and Fe<sub>2</sub>O<sub>3</sub>: a thermoanalytical investigation. *ISIJ Int* 36(9):1135–1141
39. Archana SR, Arun PS, Sreelekshmi BR, Shibli SMA (2020) Tuning of CeO<sub>2</sub>-MnO<sub>2</sub> nano composite in Al-Zn alloy matrix for effective activation. *Mater Sci Eng B: Solid-State Mater Adv Technol* 261. <https://doi.org/10.1016/j.mseb.2020.114768>
40. Dosaj et al (2014) Method and system for producing an aluminum-silicon alloy. US Pat No 8900341:B2
41. Moghadam AD, Ferguson JB, Schultz BF, Rohatgi PK (2016) In-situ reactions in hybrid aluminum alloy composites during incorporating silica sand in aluminum alloy melts. *AIMS Mater Sci* 3:954–964. <https://doi.org/10.3934/matricsci.2016.3.954>

**Publisher's Note** Springer Nature remains neutral with regard to jurisdictional claims in published maps and institutional affiliations.